Acta Pharmacologica Sinica (2014) 35: 1082–1092
 1671-4083/14 $32.00
www.nature.com/aps

Original Article

Discovery of novel aromatase inhibitors using a homogeneous time-resolved fluorescence assay

Jin-zi JI[1], Ke-jing LAO[4], Jie HU[1], Tao PANG[1, 3], Zhen-zhou JIANG[1, 2], Hao-liang YUAN[5], Jing-shan MIAO[1], Xin CHEN[1], Shan-shan NING[4], Hua XIANG[4], Yu-meng GUO[1], Ming YAN[1, 3, *], Lu-yong ZHANG[1, 6, *]

[1]Jiangsu Center for Drug Screening, China Pharmaceutical University, Nanjing 210009, China; [2]Key Laboratory of Drug Quality Control and Pharmacovigilance (China Pharmaceutical University), Ministry of Education, Nanjing 210009, China; [3]Jiangsu Center for Pharmacodynamics Research and Evaluation, China Pharmaceutical University, Nanjing 210009, China; [4]Department of Medicinal Chemistry, School of Pharmacy, China Pharmaceutical University, Nanjing 210009, China; [5]Laboratory of Molecular Design and Drug Discovery, School of Science, China Pharmaceutical University, Nanjing 210009, China; [6]State Key laboratory of Natural Medicines, China Pharmaceutical University, Nanjing 210009, China

Aim: Aromatase is an important target for drugs to treat hormone-dependent diseases, including breast cancer. The aim of this study was to develop a homogeneous time-resolved fluorescence (HTRF) aromatase assay suitable for high-throughput screening (HTS).
Methods: A 384-well aromatase HTRF assay was established, and used to screen about 7000 compounds from a compound library. Anti-proliferation activity of the hit was evaluated using alamarBlue(R) assay in a hormone-dependent breast cancer cell line T47D. Molecular docking was conducted to elucidate the binding mode of the hit using the Discovery Studio program.
Results: The *Z′* value and signal to background (S/B) ratio were 0.74 and 5.4, respectively. Among the 7000 compounds, 4 hits (XHN22, XHN26, XHN27 and triptoquinone A) were found to inhibit aromatase with IC_{50} values of 1.60±0.07, 2.76±0.24, 0.81±0.08 and 45.8±11.3 μmol /L, respectively. The hits XHN22, XHN26 and XHN27 shared the same chemical scaffold of 4-imidazolyl quinoline. Moreover, the most potent hit XHN27 at 10 and 50 μmol/L inhibited the proliferation of T47D cells by 45.3% and 35.2%, respectively. The docking study revealed that XHN27 docked within the active site of aromatase and might form a hydrogen bond and had a π-cation interaction with amino acid residues of the protein.
Conclusion: XHN27, an imidazolyl quinoline derivative of flavonoid, is a potent aromatase inhibitor with anti-proliferation activity against breast cancer *in vitro*. The established assay can be used in HTS for discovering novel aromatase inhibitor.

Keywords: aromatase; breast cancer; imidazolyl quinoline; triptoquinone A; homogeneous time-resolved fluorescence assay; high-throughput screening; molecular docking; drug discovery

Acta Pharmacologica Sinica (2014) 35: 1082–1092; doi: 10.1038/aps.2014.53; published online 21 Jul 2014

Introduction

Breast cancer is one of the most common cancers[1]. Estrogens and the estrogen receptor (ER) are well known for playing an important role in the development and progression of breast cancer[2, 3]. Aromatase is encoded by the *cyp19a1* gene[4, 5], belongs to a particular reticulum-bound cytochrome P450 superfamily and forms an electron-transfer complex with its partner, NADPH-cytochrome P450 reductase (CPR). During the aromatization reaction, electrons are transferred from NADPH, through CPR, to the heme of aromatase, then to the androgen substrate[6]. It is a rate-limiting enzyme of great importance that catalyzes the irreversible conversion of androstenedione (Δ4A) and testosterone into estrogen, estrone and estradiol (E_2)[7], thereby controlling the androgen/estrogen ratio sustaining the endocrine balance. Thus, the control of aromatase gene expression is crucial, and aromatase is becoming an important target for developing drugs to treat hormone-dependent diseases, including breast cancer, prostate cancers or other diseases related to aromatase overexpression, such as growth disorders or sexual precocity[8, 9].

Aromatase inhibitors (AIs) are continuously being developed that have considerable clinical impact on the production of estrogen among post-menopausal women and thereby on breast cancer[10, 11]. Currently, AIs are classified into two subtypes: steroidal and non-steroidal. Steroidal AIs, also

* To whom correspondence should be addressed.
E-mail brookming@163.com (Ming YAN);
lyzhang@cpu.edu.cn (Lu-yong ZHANG)
Received 2014-03-18 Accepted 2014-05-20

known as type I inhibitors and represented by formestane and exemestane, first bind to the substrate-binding site of aromatase and become a reactive intermediate that covalently binds to aromatase causing irreversible inhibition. Type II or non-steroidal AIs, covalently bind to aromatase, resulting in irreversible inhibition. Non-steroidal AIs include anastrozole, vorozole, and letrozole[12, 13]. Previous studies have demonstrated that AIs provide an increased survival benefit compared with other therapies and have acceptable toxicity profiles with decreased virginal bleeding and thromboembolism and increased rash, diarrhea and vomiting[14, 15]. As AIs sometimes have more severe bone, brain and heart side effects, research for alternative compounds is necessary[15–17].

Natural products, extracted from traditional medicines and foods, may be helpful for discovering novel AIs that may selectively target aromatase in the breast and reduce systemic toxicity[18]. Among these compounds, flavonoids[19] are the most commonly investigated agents due to their prominent aromatase inhibitory activity and high breast selectivity[18]. Moreover, flavonoids may modulate the multi-step process of carcinogenesis through cellular and molecular mechanisms[19]. Biochanin A (BCA), isolated from red clover (*Trifolium pretense*), is a common isoflavone product that can inhibit aromatase activity and cell growth in MCF-7 cells[20]. Furthermore, *cyp19a1* mRNA abundance was significantly reduced by BCA through promoter regulation in SK-BR-3 cells[20].

The classical tritiated water release assay[21, 22] is widely used to measure aromatase activity, which uses human placental microsomes or JEG-3 human choriocarcinoma cells as enzyme sources and quantifies the release of tritium from the 1β-position of Δ4A into the aqueous phase. Other aromatase assays based on high performance liquid chromatography (HPLC) separation with UV detection[23] and the fluorometric substrate, O-benzylfluorescein benzyl ester (DBF)[24], using recombinant human aromatase have also been developed to eliminate the hazards of using radiolabeled materials. However, absorbance or fluorescence interference from test compounds has restrained the HTS application of these methods. Homogeneous time-resolved fluorescence (HTRF)[25, 26] technology is an immunoassay that is based on a fluorescence resonance energy transfer (FRET) between a tris-bipyridine europium cryptate used as a long-lived fluorescent donor and a chemically modified allophycocyanin used as acceptor[27]. This technology has been documented to be a sensitive and reliable method for the HTS of diverse enzyme and receptor targets because of its reduced inter-well variation and fluorescence interference[28]. In this study, we developed an HTRF aromatase assay method and discovered several novel lead compounds that are potent aromatase inhibitors by screening a small compound library. These results will contribute to the development of novel anti-breast cancer drugs.

Materials and methods

Reagents

Human CYP19+P450 reductase supersomes were purchased from BD Biotech (CA, USA). An HTRF estradiol kit was purchased from Cisbio Bioassays (Gif-Sur-Yvette, France). β-Nicotinamide adenine dinucleotide 2′-phosphate reduced tetrasodium salt (NADPH) was acquired from Roche Applied Science (Basel, Switzerland). Testosterone, Δ4A, E_2, and letrozole were purchased from Dalian Meilun Biotech Co (Dalian, China). Dimethyl sulfoxide (DMSO), penicillin, and streptomycin were purchased from Sigma-Aldrich (MO, USA). RPMI-1640 medium, fetal bovine serum (FBS) and alamarBlue® assay kits were obtained from Life Technologies (NY, USA).

Assay development and optimization

Enzyme reactions were conducted for 1 h at 37 °C in white 384-plates (#3674, Corning, MA, USA) and then 5 μL of estradiol-XL665 conjugate and anti-estradiol cryptate conjugate (Cisbio Technologies) were added 2 h before reading the plate. Reaction volumes of 10 μL contained 15 nmol/L aromatase, 30 nmol/L testosterone and 600 nmol/L NADPH in an assay buffer consisting of 50 mmol/L potassium phosphate, pH 7.4, 0.5 mmol/L ethylenediaminetetraacetic acid (EDTA) and 5 mmol/L magnesium chloride. The enzyme reaction solution was combined with 5 μL estradiol-XL665 conjugate and 5 μL anti-estradiol cryptate diluted in reconstitution buffer (50 mmol/L phosphate buffer, pH 7.0, 0.8 mol/L KF, 0.2% BSA) in the white 384-plates mentioned above. After incubating at room temperature for 2 h, fluorescence was measured at 620 nm and 665 nm using an Envision multilabel plate reader (PerkinElmer, MA, USA) with a 100 μs delay. The HTRF ratio was defined as following: $Ratio=(Em_{665\ nm}/Em_{620\ nm})\times10^4$. Data were converted from HTRF ratio values to Delta F% via the following equation: $Delta\ F\%=[(Sample\ Ratio-Ratio_{neg})/Ratio_{neg}]\times100$. $Ratio_{neg}$ is the HTRF ratio value of the negative control (enzyme reaction replaced by 10 μL assay buffer and estradiol-XL665 by 5 μL reconstitution buffer). The EC_{80} was calculated using PRISM version 5.0 software (GraphPad Software Inc, CA, USA) from the non-linear curve fitting of the Delta F% value versus the NADPH concentration.

Determination of compound potency

Approximately 7000 compounds (10 mmol/L stock solution in DMSO) from the compound library of the National Nanjing Center for Drug Screening were plated into white 384-plates (Corning, MA, USA) using a Biomek NX^P liquid handling workstation (Beckman Coulter, CA, USA). The enzyme and the mixed solution of testosterone and NADPH diluted in buffer were added into the wells using a Multidrop reagent dispenser (Thermo Electron Corp, MA, USA) and the plates were incubated at 37 °C for 1 h. A multichannel pipette was used to add the detection reagents (5 μL estradiol-XL665 conjugate and 5 μL anti-estradiol cryptate conjugate, respectively). After incubation at room temperature for 2 h, the HTRF signals were measured using an Envision multilabel plate reader.

A hit was defined as a compound that displayed ≥50% inhibition in the primary screening. The hits selected from the primary screen were serially diluted to determine the half maximal inhibitory concentration (IC_{50}). The IC_{50} was calcu-

lated using PRISM version 5.0 software (GraphPad Software Inc, CA, USA) from the non-linear curve fitting of the Delta F% (fluorescence increasing percent) value versus the inhibitor concentration.

Analysis of assay performance

The performance of the optimized assay was evaluated by performing multiple replicate tests in a 384-well format. The *Z'* factor was calculated according to the following equation: $Z'=1-(3\times SD_{max}+3\times SD_{min})/(\mu_{max}-\mu_{min})$. SD_{max} and SD_{min} are the standard deviations of the high control (the aromatase in the enzyme reaction solution replaced by assay buffer) values and the low control (enzyme reaction solution as mentioned above) values; μ_{max} and μ_{min} are average HTRF ratio values of the high control and low control. The signal-to-background (S/B) ratio was calculated as μ_{max}/μ_{min}. Percent inhibition was calculated as the following equation: % inhibition=$(Ratio_{compound}-\mu_{neg})/(\mu_{max}-\mu_{neg})\times 100$.

Molecular docking

Molecular docking was completed using CDOCKER (Discovery Studio 2.0). CDOCKER is a grid-based molecular docking method that employs CHARMm. The receptor is held rigid while the ligands are allowed to flex during the refinement[29]. The crystal structure of aromatase (PDB code: 4KQ8, 3.29 Å) was defined as the target, and the active site of aromatase was defined according to the volume occupied by Δ4A, the known ligand crystallized in the active site. The active compound XHN27, the natural isoflavone product BCA[30] and the extensively used aromatase inhibitor, letrozole, were docked into the active site of aromatase to determine their preferential conformations. During the docking process, the top 10 conformations were generated for each ligand based on the docking score after energy minimization using the smart minimizer method, which begins with the steepest descent method followed by the conjugate gradient method. For each final pose, the CHARMm energy and the interaction energy are calculated. The poses are sorted by CHARMm energy and the 10 top scoring poses are retained[31]. The binding modes were validated by the hydrogen bond interactions and π-π interactions between the candidate molecules and active site residues.

Cell proliferation assay

T47D cells were maintained in RPMI-1640 medium containing 10% FBS, 100 U/mL penicillin and 100 μg/mL streptomycin, grown at 37 °C in 5% CO_2. Before treatment with test compounds, cells were steroid deprived using RPMI-1640 supplemented with 10% charcoal-stripped FBS for 3 d. Because T47D is an ER-positive breast cancer cell line that increases cell proliferation in response to estrogen[32], the inhibition induced by the test compounds on this cell line is ascribed to their aromatase inhibition activity. For the cell proliferation assay, cells were seeded into 96-well black clear-bottom plates (10 000 cells per well) and allowed to attach overnight. Cells were treated with 10 nmol/L Δ4A or 1 nmol/L E_2 and various concentrations of test compounds (0.2, 1, 3, 10, and 50 μmol/L) for 3 d or 6 d. Each concentration was tested in triplicate. The proliferation assay was performed using the alamarBlue® assay as previously described[33, 34]. A Safire^2 microplate reader (Tecan, Switzerland) was used to detect the fluorescent intensity at Ex 560 nm/Em 590 nm. The inhibition rate was calculated using the following formula: % inhibition=$[1-(RFU_{sample}-RFU_{blank})/(RFU_{negative}-RFU_{blank})]\times 100$. RFU_{sample}, RFU_{blank}, and $RFU_{negative}$ are the fluorescent intensity of the sample wells, control wells without cells and negative control wells containing 0.5% DMSO, respectively.

Statistical analysis

The data from the inhibition assays were analyzed from the non-linear curve fitting of the Delta F% value versus the inhibitor concentration using PRISM version 5.0 software (GraphPad Software Inc, CA, USA). Data are expressed as the mean±SEM. The significance of differences between groups were evaluated using a one-way analysis of variance (ANOVA) followed by a Dunnett multiple comparison post-test. Differences were considered to be statistically significant at $P<0.05$.

Results

Establishment of a 384-well HTRF aromatase assay

A 384-well aromatase HTRF assay was established by quantifying estradiol production during the aromatase reaction. This detection method relies on competitive binding of exogenous, free estradiol disrupting the donor-acceptor complex. Therefore, the observed HTRF signal decreased with increasing amounts of product estradiol (Figure 1A and 1B). As it is typical for HTRF, the long lifetime of the donor fluorophore employed minimizes fluorescence interference due to buffers or test compounds.

To define the standard titration for testosterone, the K_m of the substrate was estimated. Because there is cross reactivity between testosterone and estradiol, testosterone (>150 nmol/L) could interfere with estradiol detection in our assay (Figure 2A). The velocity was plotted as a function of testosterone concentration, and the K_m of testosterone was calculated using the Michaelis-Menten equation (Figure 2B). The calculated K_m of testosterone was 23.37±4.67 nmol/L, which corresponds to data reported in previous studies[24]. To allow for IC_{50} measurements of a similar magnitude K_i for competitive inhibitors, we selected an optimized assay condition of 30 nmol/L testosterone.

To determine the optimal condition for estradiol measurements, the time-dependence of enzyme activity and dose-dependence of NADPH were examined. Reaction progression curves were generated at several enzyme concentrations using the HTRF assay (Figure 2C). Reaction conditions with aromatase at 15 nmol/L for 60 min were then used to determine the optimal NADPH concentration. The plots of Delta F% as a function of the concentration of NADPH indicated that 600 nmol/L was appropriate for our assay (Figure 2D).

Because all compounds were dissolved in DMSO, the effect

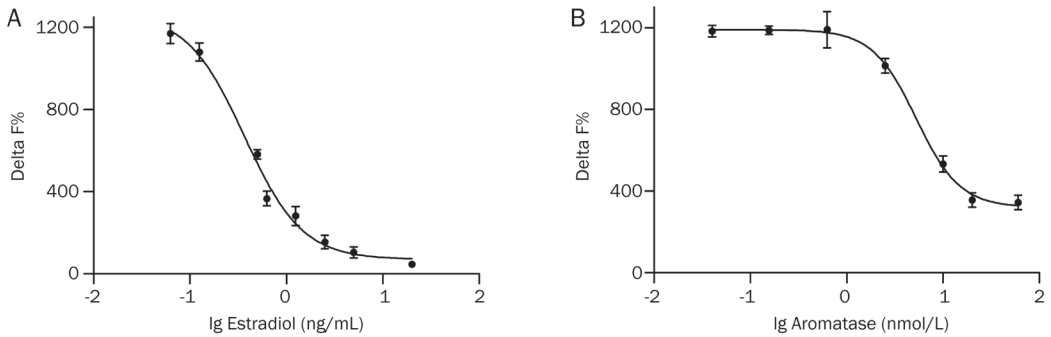

Figure 1. The application of HTRF estradiol detection method in determining aromatase activity. (A) The standard curve of estradiol was generated from increasing the concentration of the standard. Estradiol was detected by the binding of homogenous time-resolved fluorescence (HTRF) donor anti-estradiol antibody conjugated with cryptate to d 2 acceptor conjugated estradiol, producing a time-resolved fluorescence resonance energy transfer signal. Enzyme-produced estradiol competes with this interaction and reduces overall time-resolved fluorescence resonance energy transfer signals. (B) The concentration-responsive curve of aromatase was generated by adding 30 nmol/L testosterone, 1 μmol/L NADPH and increasing amount of aromatase from 0.04 nmol/L to 60 nmol/L in the reaction system. The detection buffer was added after incubation for 1 h at 37 °C. Values are represented as mean±SEM of three independent experiments (n=3).

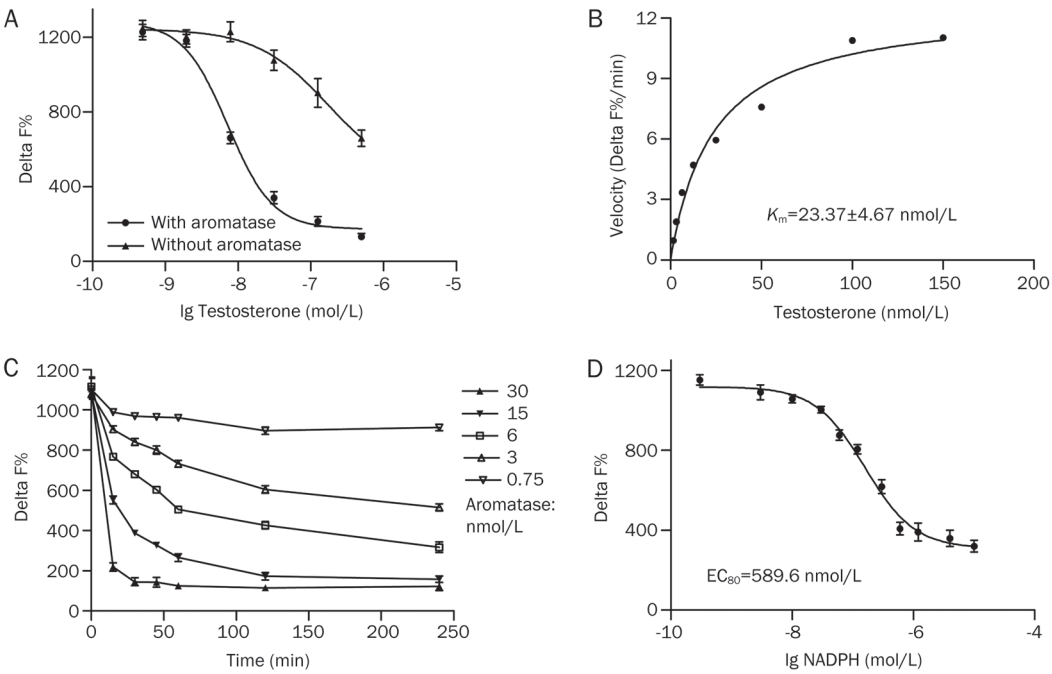

Figure 2. The optimal concentrations of substrate, enzyme and co-factor NADPH were determined. (A) The HTRF signals generated by increasing amount of testosterone in the presence and absence of 15 nmol/L aromatase. (B) Michaelis-Menton plots of aromatase activity as a function of the concentration of the substrate testosterone. (C) Time course at various concentrations of aromatase. The detection time was set at 0, 15, 30, 45, 60, 120, and 240 min. (D) Activity of aromatase was raised with the increasing concentration of NADPH (0.3 nmol/L to 10 000 nmol/L). Values are represented as mean±SEM of three independent experiments (n=3).

of DMSO concentration on the aromatase assay was examined. It was found that this assay had a high DMSO tolerance. The DMSO concentration was less than 1% during testing and has no significant effect on the Delta F% in the assays.

Determination of assay performance

To characterize the assay variability in the 384-well plate, an automated liquid handling system was employed including a Multidrop (Thermo Electron Corp, MA, USA) and Biomek NX^P (Beckman Coulter, CA, USA). The wells in column 1 were used as minimal controls and those in column 2 as maximal controls. The Z' factor is a parameter defined to reflect data variation and is widely used to assess assay quality for high-throughput screening[35]. The Z' factor for this aroma-

tase HTRF assay was 0.74±0.02, and the signal-to-background (S/B) ratio was 5.40±0.18, indicating that the assay was reliable for high-throughput screening.

To further test the utility of the HTRF assay for measuring inhibitor potency, the IC_{50} value of letrozole, a known inhibitor of aromatase, was determined. Letrozole was dissolved in DMSO to make a stock solution of 10 mmol/L, and the solution was serially diluted using assay buffer. A representative concentration-response curve of letrozole was plotted using PRISM version 5.0 software (GraphPad Software Inc, CA, USA) (Figure 3A), and IC_{50} value was 26.0±6.6 nmol/L, which coincides with previously reported data[36–38]. Our results indicate that the aromatase HTRF assay is a potentially robust assay that can be used to determine the potency of aromatase inhibitors.

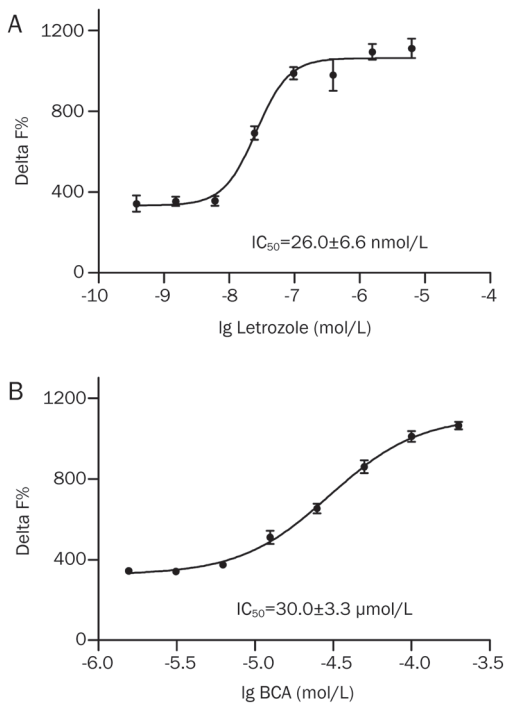

Figure 3. HTRF assay verification. (A) HTRF signal in the presence of known aromatase inhibitors, letrozole. Lines shown are fits giving IC_{50} of 26.0±6.6 nmol/L. (B) BCA is isoflavone natural product. Lines shown are fits giving IC_{50} of 30.0±3.3 μmol/L. Values are represented as mean±SEM of three independent experiments (n=3).

Application of the aromatase HTRF assay for screening

Compounds were tested at a single concentration of 0.1 mmol/L in duplicate. The primary screening was performed with 15 nmol/L aromatase, 30 nmol/L testosterone, and 600 nmol/L NADPH and resulted in 5 hits. The secondary screening resulted in 4 confirmed hits, XHN22, XHN26, XHN27, and triptoquinone A (TQA) (Figure 4A–4D), representing a hit rate of 0.067%. Three of the 4 compounds (XHN22, XHN26 and XHN27), derivatives of flavone, share the general chemical skeleton of imidazolyl quinoline (Figure 5) and had an IC_{50} against aromatase of 1.60±0.07 μmol/L, 2.76±0.24 μmol/L, and 0.81±0.08 μmol/L, respectively (Figure 4A–4C). The IC_{50} of biochanin A (BCA) was 30.0±3.3 μmol/L (Figure 3B), indicating that BCA possesses a relatively weak activity against aromatase compared with the imidazolyl quinoline derivatives discovered in this study. The other confirmed hit, TQA (Figure 4D), extracted from *Tripterygium wilfordii*, was less potent compared with XHN27 (Figure 4C), with an IC_{50} against aromatase of 45.8±11.3 μmol/L.

Evaluation of selected hits to inhibit cell proliferation rates

To examine the pharmacological properties of the hit compounds on aromatase, cell proliferation assays were performed. T47D cells were treated with Δ4A and increasing concentrations of XHN27, BCA or letrozole for 3 d and 6 d, and the inhibition of cell proliferation was evaluated using the alamarBlue® assay. Letrozole was a more potent inhibitor of cell proliferation than XHN27 and BCA (Figure 6A, 6B). The inhibition rate of letrozole (3 μmol/L) was 54.6% after 6 d (Figure 6B), while XHN27 at 50 μmol/L was 45.3%, and 35.2% at 10 μmol/L. Moreover, XHN27 exhibited increased cytotoxicity against T47D cells compared with BCA, which inhibited T47D cell proliferation by 30.6% at 50 μmol/L and 18.7% at 10 μmol/L after 6 d.

To address whether reduction in cell viability was due to aromatase inhibition, we evaluated the effects of compounds on estradiol (E_2)-treated T47D cells for the same periods of time as for Δ4A-treated cells. As presented in Figure 6C and 6D, exogenous E_2 was able to rescue the anti-proliferation effects of 3, 10, and 50 μmol/L XHN27 on T47D cells following treatment for 6 d when compared with co-treatment with Δ4A and XHN27. The inhibition rates decreased from 45.3% in Δ4A-treated cells to 24.4% in E_2-treated cells after administration with 50 μmol/L XHN27 for 6 d, from 35.2% to 19.6% after administration with 10 μmol/L XHN27, and from 24.6% to 7.7% after administration with 3 μmol/L XHN27. These results indicated that XHN27 inhibited T47D cell proliferation through aromatase inhibition.

Analysis of XHN27 binding mode

XHN27 was discovered to possess the best aromatase inhibitory activity among the selected hit compounds and had pharmacological properties against breast cell proliferation in our previous assay. To clarify the binding mode of XHN27 with aromatase compared with letrozole and BCA, these three molecules were docked into the active site of aromatase. The crystal structure of the enzyme was obtained from the Protein Data Bank (PDB). According to previous literature[39], the residues comprising the catalytic cleft are Ile 305, Ala 306, Asp 309 and Thr 310, Phe 221, Trp 224, Ile 133, Phe 134, Val 370, Leu 372, Val 373, Met 374, Leu 477, and Ser 478.

The 22-nitrile and 20-nitrile of letrozole form two hydrogen bonds with the hydroxyl of Ser 478 and the amide of Met 374, respectively (Figure 7A). Unlike the binding mode of Δ4A with the Fe atom of the heme group, the triazole of letrozole forms a π–π stacking interaction with the porphyrin ring and

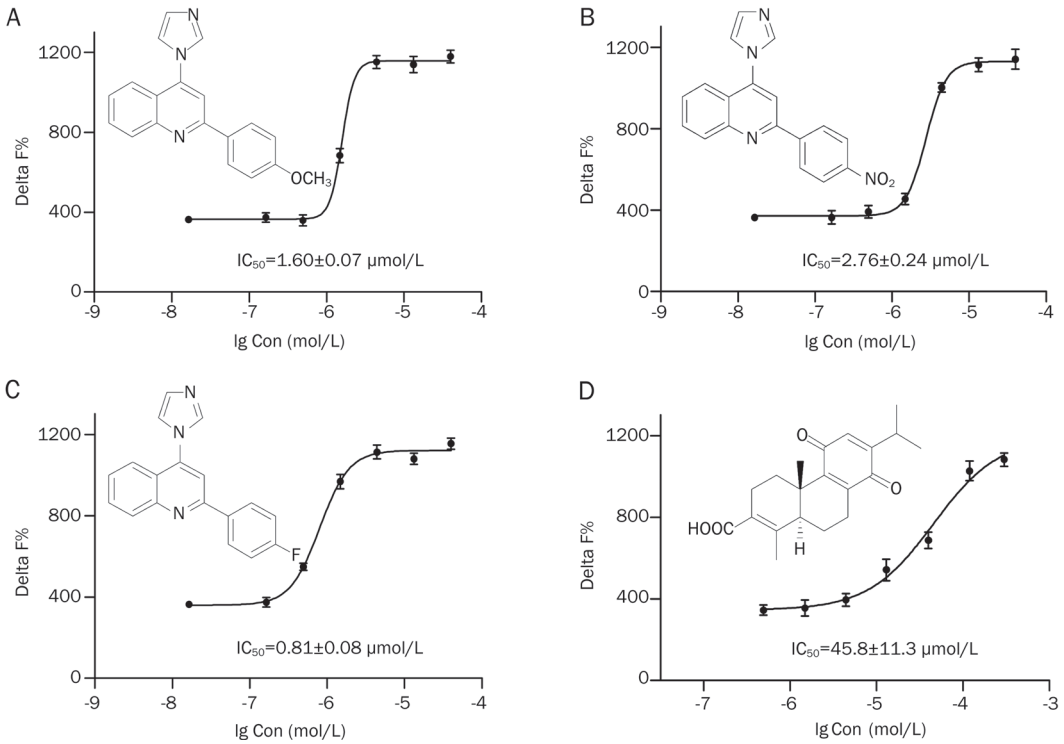

Figure 4. Three flavone derivatives, XHN22, XHN26, XHN27 (A, B, C) and the active principal of *Triptergium wilfordii*, TQA (D) are potent inhibitors of aromatase activities. Lines shown are fits of these four inhibitors giving IC_{50} of 1.60±0.07 μmol/L, 2.76±0.24 μmol/L, 0.81±0.08 μmol/L, and 45.8±11.3 μmol /L, respectively. Values are represented as mean±SEM of three independent experiments (*n*=3).

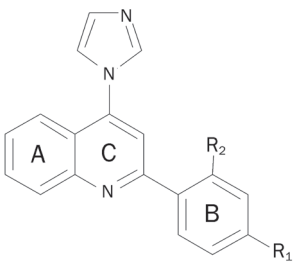

Figure 5. The skeleton of the newly discovered aromatase inhibitor.

a π-cation interaction with the Fe atom (Figure 8A), which may explain its affinity for the enzyme. Furthermore, one of the benzonitrile groups extended into the access channel that links the active site to the outer surface. Thus, letrozole would tightly bind in the pocket instead of Δ4A.

Similar to exemestane, the A-ring of BCA is accommodated in a hydrophobic crevice surrounded by the side-chain C atoms of Thr 310, Val 370, and Ser 478 (Figure 7B). However, the two hydroxyl groups in the A-ring and the adjacent carboxyl group of the C-ring may attenuate the hydrophobic interaction between them. The B-ring failed to be accommodated in the pocket surrounded by Ile 133, Phe 134, Leu 372, Val 373, and Met 374 (Figure 7B). Moreover, the methoxy in the B-ring provides low affinity with the side chains of Phe 134, Leu 372, and Met 374, ascribed to steric factors. However, the π-π stacking interaction between the A-ring, C-ring, and benzene ring of Trp 224, together with the interaction between the B-ring and Phe 134 (Figure 8B), strengthen the binding of BCA into the active site.

The docking conformation of XHN27 conforms to the binding pocket of aromatase and forms key hydrogen bonds between its 4′-F and the amide of Met 374 and the NH- of Arg 115 (Figure 7C). The A-ring and 4-imidazolyl are near Asp 309 and Thr 310, which form the catalytic cleft of the enzyme and provide van der Waals contacts with the side chains of these amino acids that extend into the access channel (Figure 7C). The B-ring is accommodated in the pockets, which consist of Leu 372, Val 373, and Met 374, and the hydrogen bonds provide strong contact with them. Moreover, a π-cation interaction is observed between the C-ring and the porphyrin rings (Figure 8C).

Discussion

Increasing evidence suggests that non-steroid AIs[40] are highly specific, potent and have less adverse effects during breast cancer treatment. These AIs such as anastrozole and letrozole[41, 42], by non-covalently binding to the aromatase enzyme heme moiety and preventing androgen binding by saturating the binding site, are a successful alternative to tamoxifen as a first-line therapy in postmenopausal women. However, several clinical trials in postmenopausal breast cancer patients and healthy postmenopausal women treated with AIs evalu-

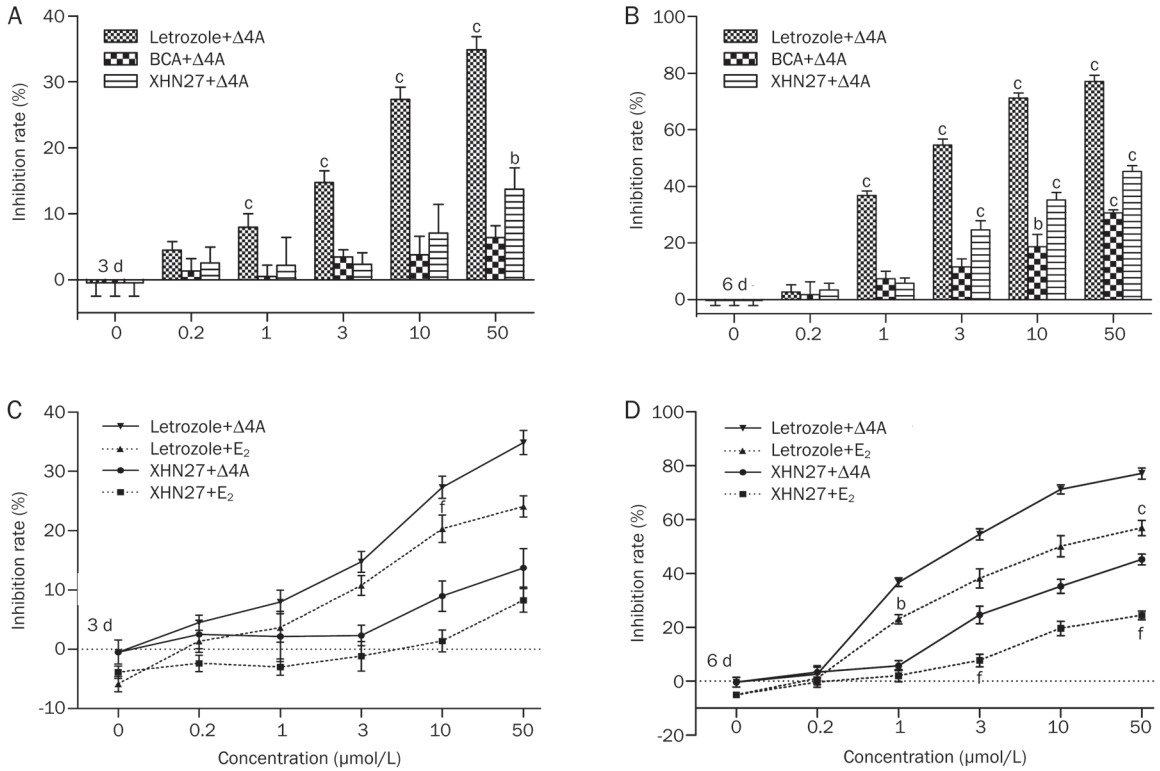

Figure 6. Effects of letrozole, BCA, and XHN27 on the proliferation of T47D cell cultured with 10 nmol/L Δ4A (A, B) or 1 nmol/L E_2 (C, D). Cells were cultured with different concentrations of each compound (0.2–50 μmol/L) for 3 d (A, C) or 6 d (B, D). Values are represented as mean±SEM of three independent experiments (n=3). Significant differences between the compounds-treated groups versus negative control are denoted by $^bP<0.05$, $^cP<0.01$. One-way ANOVA followed by Dunnett multiple comparison post-test. Significant differences between the E_2-treated cells (dashed lines) versus Δ4A-treated cells (solid lines) after administration with XHN27 are denoted by $^bP<0.05$, $^cP<0.01$. Significant differences between the E_2-treated cells versus Δ4A-treated cells after administration with letrozole are denoted by $^eP<0.05$, $^fP<0.01$.

ated the risks of bone fractures. A clinical trial that evaluated the effects of anastrozole, letrozole and exemestane on bone health demonstrated that after 24 weeks of treatment, all 3 inhibitors caused increased bone resorption and decreased bone formation[43].

Methods for characterizing aromatase activity that are amenable to HTS may serve as tools to investigate new compounds with less therapeutic risks. However, few such methods have been described. Both human placental microsome-based assays and cell-based assays employ tritiated Δ4A to measure aromatase activity. However, these methods require strict experimental environments and are not amenable for screening large compound libraries[23, 44]. Moreover, the purified aromatase used in our assay may avoid many of the variables that affect compound performance on target binding and signal reading such as cell membrane permeability, serum stability, plasma protein binding, and the interference of other microsome enzymes in catalyzing the substrate.

Here, we reported a rational approach for discovering novel aromatase inhibitors with a robust HTRF detection method that avoids the limitations of currently available methods[23, 24, 45]. The detection signal is inversely proportional to the estradiol concentration because the HTRF detection method is a competition assay. Because the detection signal of the aromatase reaction was almost confined to the linear range of estradiol variation and the concentration of the catalytic product would not exceed 10 ng/mL in the presence of 30 nmol/L substrate, the raw signal provides a representative estradiol concentration. Therefore, we plotted the curves against the calculated Delta F%.

In the kinetic assay of aromatase activity, the signals within different time courses were collected. The optimal aromatase amount was determined to be 0.15 pmol/well; resulting in a promising detection window. Moreover, we demonstrated a linear decrease in Delta F% with increasing incubation time within 1 h. It was confirmed that the aromatase reaction required cofactor NADPH as hydrogen donor and the NADPH-response curve demonstrated comparable enzyme activity between 600 nmol/L and 3 μmol/L. Therefore, the EC_{80} of 600 nmol/L NADPH was used as a standard condition in our assay. The substrate dose-response curve indicated that when testosterone was used at concentrations above 100 nmol/L, the fluorescent signal may have experienced interference due to excessive substrate for the analogical structures of estradiol and testosterone. However, the Michaelis-Menten fit of the reaction velocity as a function of the substrate resulted in an approximate K_m value less than 30 nmol/L for testosterone, which was in agreement with an earlier reported value

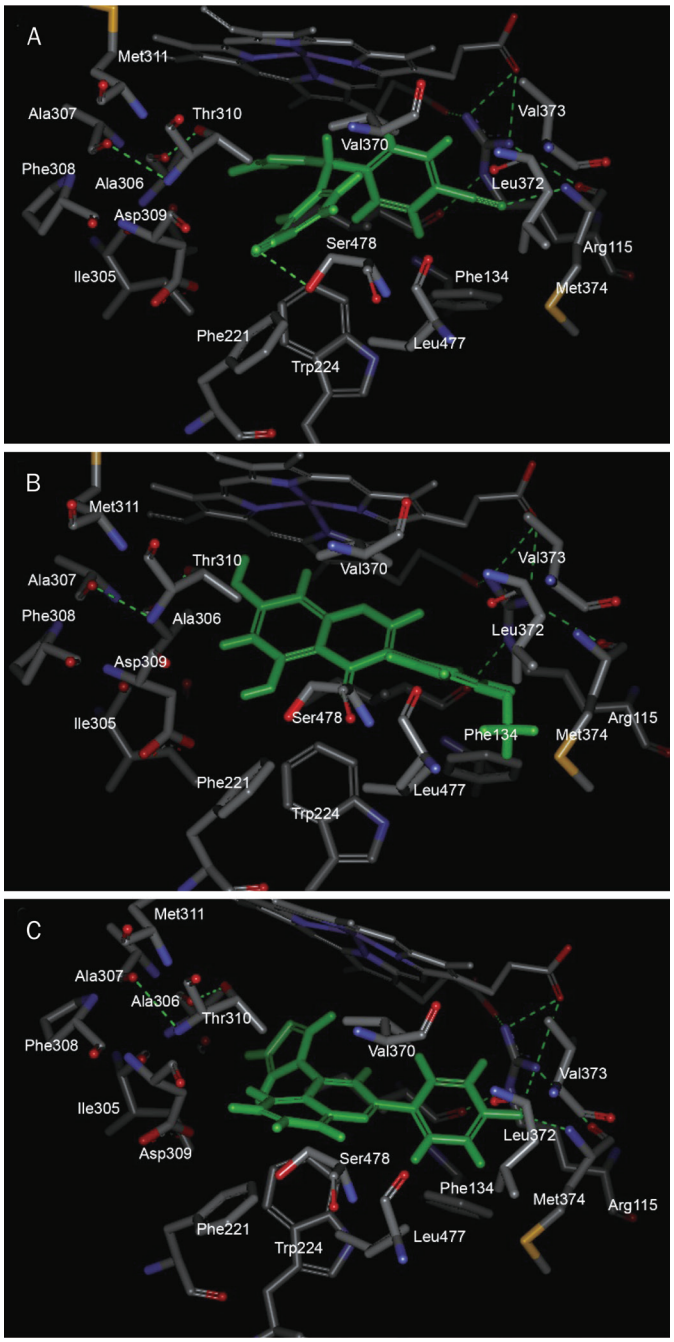

Figure 7. Binding mode of letrozole (A), BCA (B) and XHN27 (C) in crystal structure of aromatase (PDB code: 4KQ8). Hydrogen bonds are shown as dashed green lines. Carbon atoms, oxygen atoms, nitrogen atoms and sulfur atoms are shown as grey, red, blue, and yellow, respectively.

of 40 nmol/L[24]. Thus, the optimized assay condition of 30 nmol/L testosterone was selected in our protocol.

Furthermore, we determined the sensitivity of our method by testing the widely used aromatase inhibitor letrozole. The IC_{50} value of letrozole was 30 nmol/L, in accordance with the literature data (0.67 nmol/L)[46], indicating that this aromatase assay was comparable with the conventional human placen-

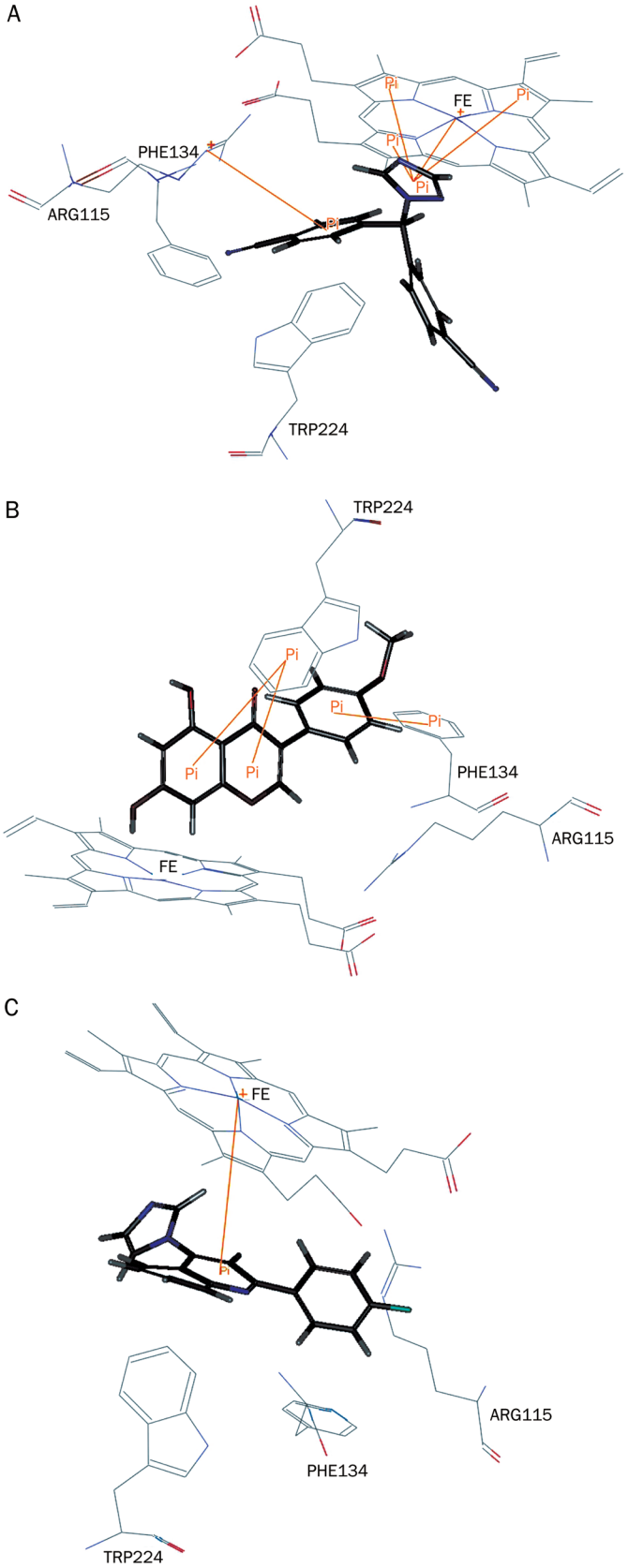

Figure 8. π-π stacking interactions of the compounds letrozole (A), BCA (B), and XHN27 (C) with the side chains of amino acid residues of aromatase.

tal microsome methods. Subsequently, the high-throughput aromatase assay was utilized to screen a compound library of 7000 samples for identifying aromatase inhibitors. The HTS aromatase assay demonstrated a robust performance with a Z' factor equal to 0.72 and S/B ratio of 5.27[35].

Five hits were chosen based on their inhibition rate in the primary screening, and 4 lead compounds were confirmed in the secondary screening. These compounds belong to 2 chemical classes – flavone derivatives and diterpenoid alkaloid natural products. Among the verified hits, XHN27 was the most potent aromatase inhibitor. To explore the effect of XHN27 on breast cells, a cell proliferation assay was conducted. T47D is an ER-positive breast cancer cell line that demonstrates increased cell proliferation in response to estrogen[32] and was considered to be a suitable model for this investigation because it has been reported that T47D cells have the unique capacity to convert *de novo* [^{14}C]androstenedione into radioactive estrone and estradiol[47]. Letrozole was used as a positive control for aromatase inhibition[48]. This study demonstrated that XHN27 exhibits promising inhibitory action against breast cancer, better than BCA, and XHN27 may be a promising aromatase inhibitor candidate. As T47D cells are an ER-positive[49] and aromatase-expressing[50, 51] breast cancer cell line, aromatase inhibition and lack of estrogen after XHN27 administration may be lethal to these cells. However, the cytotoxicity of XHN27 and the *cyp19* gene expression profile after treatment remain to be investigated.

To explore the mechanism of XHN27 aromatase inhibition, this compound, letrozole and BCA were computationally docked into the aromatase active site. We discovered that XHN27 exhibited a different binding mode compared with letrozole. In addition to the lack of an electron-donating group in the A-ring, which made the π-π connection to heme iron impossible, an opposite conformation of 4-imidazolyl with porphyrin rings indicated a much weaker interaction than that between the triazole of letrozole and the porphyrin rings. This explains why letrozole more potently inhibits aromatase activity. However, the B-ring formed hydrogen bonds with Met 374 and Arg 115. The docking results demonstrated that the 22-nitrile of letrozole formed hydrogen bonds with Met 374, indicating that electronegativity was important for the tight binding with aromatase, along with steric factors.

Thus, we concluded that XHN27 was the most potent among the three imidazolyl quinoline derivatives of flavone due to electronic and steric factors. The 4-nitryl of XHN26 was sterically bulky and the 4- methoxy of XHN22 was less electronegative. Moreover, the π-cation interaction between the C-ring and porphyrin rings may enhance the forces, suggesting that XHN27 exhibits a potent inhibitory action. It was considered that the isoflavone ring skeleton was inappropriate for the development of aromatase inhibitors because of its poor inhibition potency[52]. In accordance with this, we demonstrated during molecular docking that the B-ring of isoflavone BCA failed to be accommodated within the aromatase active pocket. However, by replacing the electron-donating group, the imidazolyl with a 4-carbonyl in the C-ring, the imidazolyl quinoline derivatives of flavone proved to be more potent aromatase inhibitors compared with BCA. Furthermore, the substitute of quinoline for the chromone nucleus of flavone would improve structural stability, which is important for drug development. Although competitive inhibition assays were not included in this study, it was speculated during the molecular docking study that XHN27 may be a competitive aromatase inhibitor. It was observed during docking that the interactions between XHN27 and aromatase included a hydrophobic interaction, hydrogen bond and π-cation connection. The lack of a covalent bond between 4-imidazolyl and heme iron due to the opposite conformation may indicate that the interaction was competitive and reversible.

In conclusion, we have developed an HTRF-based aromatase assay for high-throughput screening with a reasonable S/B ratio and Z' factor. Using this assay, we discovered two classes of compounds, flavone derivatives and diterpenoid alkaloid natural products, confirmed the anti-proliferation effects of the most potent compound, XHN27 and delineated the structure–activity relationship for this compound. Further investigations on this compound should include diverse approaches such as the evaluation of its effects on other steroid receptors or enzymes, analysis of its metabolic stability, assessment of its toxicity and chemical modification for higher potency.

Acknowledgements

This project was supported by "National Natural Science Foundation of China" (No 81102876, 81373179); Major Scientific and Technological Special Project for Significant New Drugs Creation (No 2012ZX09504001-001); Jiangsu Province Science and Technology Support Program of Social Development Projects (BE2012745); and this study was partially supported by the 111 Project (111-2-07). Thanks to Mr Peng GAO for assistance with the experiments, Mounia GUERRAM for revision in language of the manuscript, and Dr Ya-dong CHEN for valuable suggestions.

Author contribution

Jin-zi JI, Ming YAN, and Lu-yong ZHANG designed research; Jie HU, and Jin-zi JI performed research; Jing-shan MIAO, Xin CHEN, and Yu-meng GUO contributed the cell proliferation assay; Ke-jing LAO, Shan-shan NING, and Hua XIANG performed the structure-activity study; Hao-liang YUAN and Jin-zi JI performed the molecular docking; Jin-zi JI, Tao PANG, and Zhen-zhou JIANG wrote the paper.

Abbreviation

AG, aminoglutethimide; AIs, aromatase inhibitors; BCA, biochanin A; BSA, albumin from bovine serum; *cyp19a1*, aromatase gene; DBF, *O*-benzylfluorescein benzyl ester; Delta F%, fluorescence increasing percent; DMSO, dimethyl sulfoxide; EC_{80}, concentration for 80% of maximal effect; EDTA, ethylene diamine tetraacetic acid; ER, estrogen receptor; FBS, fetal bovine serum; FRET, fluorescence resonance energy transfer; HPLC, high performance liquid chromatography; HTRF,

homogeneous time-resolved fluorescent; HTS, high-throughput screening; IC_{50}, half maximal inhibitory concentration; KF, potassium fluoride; NADPH, β-nicotinamide adenine dinucleotide 2′-phosphate reduced tetrasodium salt; TQA, triptoquinone A; Δ4A, androstenedione.

References

1 Igene H. Global health inequalities and breast cancer: an impending public health problem for developing countries. Breast J 2008; 14: 428–34.
2 Tian CY, Hu CQ, Xu G, Song HY. Assessment of estrogenic activity of natural compounds using improved E-screen assay. Acta Pharmacol Sin 2002; 23: 572–6.
3 Raina K, Agarwal R. Combinatorial strategies for cancer eradication by silibinin and cytotoxic agents: efficacy and mechanisms. Acta Pharmacol Sin 2007; 28: 1466–75.
4 Means GD, Mahendroo MS, Corbin CJ, Mathis JM, Powell FE, Mendelson CR, *et al.* Structural analysis of the gene encoding human aromatase cytochrome P-450, the enzyme responsible for estrogen biosynthesis. J Biol Chem 1989; 264: 19385–91.
5 Chen SA, Besman MJ, Sparkes RS, Zollman S, Klisak I, Mohandas T, *et al.* Human aromatase: cDNA cloning, Southern blot analysis, and assignment of the gene to chromosome 15. DNA 1988; 7: 27–38.
6 Hong Y, Li H, Yuan YC, Chen S. Sequence-function correlation of aromatase and its interaction with reductase. J Steroid Biochem Mol Biol 2010; 118: 203–6.
7 Cheng HH, Hu XJ, Ruan QR. Dehydroepiandrosterone anti-atherogenesis effect is not via its conversion to estrogen. Acta Pharmacol Sin 2009; 30: 42–53.
8 Feuillan P, Merke D, Leschek EW, Cutler GB Jr. Use of aromatase inhibitors in precocious puberty. Endocr Relat Cancer 1999; 6: 303–6.
9 Roth C, Freiberg C, Zappel H, Albers N. Effective aromatase inhibition by anastrozole in a patient with gonadotropin-independent precocious puberty in McCune-Albright syndrome. J Pediatr Endocrinol Metab 2002; 15 Suppl 3: 945–8.
10 Gao Q, Patani N, Dunbier AK, Ghazoui Z, Zvelebil M, Martin LA, *et al.* Effect of aromatase inhibition on functional gene modules in oestrogen receptor positive breast cancer and their relationship with antiproliferative response. Clin Cancer Res 2014; 20: 2485–94.
11 Henry NL, Conlon A, Kidwell KM, Griffith K, Smerage JB, Schott AF, *et al.* Effect of estrogen depletion on pain sensitivity in aromatase inhibitor-treated women with early-stage breast cancer. J Pain 2014; 15: 468–75.
12 Lombardi P. Exemestane, a new steroidal aromatase inhibitor of clinical relevance. Biochim Biophys Acta 2002; 1587: 326–37.
13 Dutta U, Pant K. Aromatase inhibitors: past, present and future in breast cancer therapy. Med Oncol 2008; 25: 113–24.
14 Chlebowski R, Cuzick J, Amakye D, Bauerfeind I, Buzdar A, Chia S, *et al.* Clinical perspectives on the utility of aromatase inhibitors for the adjuvant treatment of breast cancer. Breast 2009; 18: S1–S11.
15 Bao T, Cai L, Snyder C, Betts K, Tarpinian K, Gould J, *et al.* Patient-reported outcomes in women with breast cancer enrolled in a dual-center, double-blind, randomized controlled trial assessing the effect of acupuncture in reducing aromatase inhibitor-induced musculoskeletal symptoms. Cancer 2014; 120: 381–9.
16 Pouliot L, Schneider M, DeCristofaro M, Samadfam R, Smith SY, Beckman DA. Assessment of a nonsteroidal aromatase inhibitor, letrozole, in juvenile rats. Birth Defects Res B Dev Reprod Toxicol 2013; 98: 374–90.
17 Bian C, Zhao Y, Guo Q, Xiong Y, Cai W, Zhang J. Aromatase inhibitor letrozole downregulates steroid receptor coactivator-1 in specific brain regions that primarily related to memory, neuroendocrine and integration. J Steroid Biochem Mol Biol 2014; 141C: 37–43.
18 Balunas MJ, Kinghorn AD. Natural compounds with aromatase inhibitory activity: an update. Planta Med 2010; 76: 1087–93.
19 Li QY, Chen L, Zhu YH, Zhang M, Wang YP, Wang MW. Involvement of estrogen receptor-beta in farrerol inhibition of rat thoracic aorta vascular smooth muscle cell proliferation. Acta Pharmacol Sin 2011; 32: 433–40.
20 Wang Y, Man Gho W, Chan FL, Chen S, Leung LK. The red clover (Trifolium pratense) isoflavone biochanin A inhibits aromatase activity and expression. Br J Nutr 2008; 99: 303–10.
21 Lephart ED, Simpson ER. Assay of aromatase activity. In: Waterman MR, Johnson EF, editors. Methods in enzymology. Orlando: Academic Press; 1991. p 477–83.
22 Ros AF, Franco AM, Groothuis TG. Experience modulates both aromatase activity and the sensitivity of agonistic behaviour to testosterone in black-headed gulls. Physiol Behav 2009; 97: 30–5.
23 Trosken ER, Fischer K, Volkel W, Lutz WK. Inhibition of human CYP19 by azoles used as antifungal agents and aromatase inhibitors, using a new LC-MS/MS method for the analysis of estradiol product formation. Toxicology 2006; 219: 33–40.
24 Stresser DM, Turner SD, McNamara J, Stocker P, Miller VP, Crespi CL, *et al.* A high-throughput screen to identify inhibitors of aromatase (CYP19). Anal Biochem 2000; 284: 427–30.
25 Chen S, Chen LL, Luo HB, Sun T, Chen J, Ye F, *et al.* Enzymatic activity characterization of SARS coronavirus 3C-like protease by fluorescence resonance energy transfer technique. Acta Pharmacol Sin 2005; 26: 99–106.
26 Mao WF, Shao MH, Gao PT, Ma J, Li HJ, Li GL, *et al.* The important roles of RET, VEGFR2 and the RAF/MEK/ERK pathway in cancer treatment with sorafenib. Acta Pharmacol Sin 2012; 33: 1311–8.
27 Ha T, Enderle T, Ogletree DF, Chemla DS, Selvin PR, Weiss S. Probing the interaction between two single molecules: fluorescence resonance energy transfer between a single donor and a single acceptor. Proc Natl Acad Sci U S A 1996; 93: 6264–8.
28 Degorce F, Card A, Soh S, Trinquet E, Knapik GP, Xie B. HTRF: A technology tailored for drug discovery — a review of theoretical aspects and recent applications. Curr Chem Genomics 2009; 3: 22–32.
29 Chen YC, Liu YL, Li FY, Chang CI, Wang SY, Lee KY, *et al.* Antcin A, a steroid-like compound from *Antrodia camphorata*, exerts anti-inflammatory effect via mimicking glucocorticoids. Acta Pharmacol Sin 2011; 32: 904–11.
30 Ma HR, Wang J, Qi HX, Gao YH, Pang LJ, Yang Y, *et al.* Assessment of the estrogenic activities of chickpea (*Cicer arietinum* L) sprout isoflavone extract in ovariectomized rats. Acta Pharmacol Sin 2013; 34: 380–6.
31 Chen CY, Chang YH, Bau DT, Huang HJ, Tsai FJ, Tsai CH, *et al.* Discovery of potent inhibitors for phosphodiesterase 5 by virtual screening and pharmacophore analysis. Acta Pharmacol Sin 2009; 30: 1186–94.
32 Dowsett M, Macaulay V, Gledhill J, Ryde C, Nicholls J, Ashworth A, *et al.* Control of aromatase in breast cancer cells and its importance for tumor growth. J Steroid Biochem Mol Biol 1993; 44: 605–9.
33 Voytik-Harbin SL, Brightman AO, Waisner B, Lamar CH, Badylak SF. Application and evaluation of the alamarBlue assay for cell growth and survival of fibroblasts. *In Vitro* Cell Dev Biol Anim 1998; 34: 239–46.
34 Chen CC, Chen HL, Hsieh CW, Yang YL, Wung BS. Upregulation of NF-

E2-related factor-2-dependent glutathione by carnosol provokes a cytoprotective response and enhances cell survival. Acta Pharmacol Sin 2011; 32: 62–9.

35 Zhang JH, Chung TD, Oldenburg KR. A simple statistical parameter for use in evaluation and validation of high throughput screening assays. J Biomol Screen 1999; 4: 67–73.

36 Kim YW, Hackett JC, Brueggemeier RW. Synthesis and aromatase inhibitory activity of novel pyridine-containing isoflavones. J Med Chem 2004; 47: 4032–40.

37 Wood PM, Woo LWL, Humphreys A, Chander SK, Purohit A, Reed MJ, *et al.* A letrozole-based dual aromatase-sulphatase inhibitor with *in vivo* activity. J Steroid Biochem Mol Biol 2005; 94: 123–30.

38 Bhatnagar AS, Hausler A, Schieweck K, Lang M, Bowman R. Highly selective inhibition of estrogen biosynthesis by CGS 20267, a new non-steroidal aromatase inhibitor. J Steroid Biochem Mol Biol 1990; 37: 1021–7.

39 Ghosh D, Griswold J, Erman M, Pangborn W. Structural basis for androgen specificity and oestrogen synthesis in human aromatase. Nature 2009; 457: 219–23.

40 Geisler J, Haynes B, Anker G, Dowsett M, Lonning PE. Influence of letrozole and anastrozole on total body aromatization and plasma estrogen levels in postmenopausal breast cancer patients evaluated in a randomized, cross-over study. J Clin Oncol 2002; 20: 751–7.

41 Murray J, Young OE, Renshaw L, White S, Williams L, Evans DB, *et al.* A randomised study of the effects of letrozole and anastrozole on oestrogen receptor positive breast cancers in postmenopausal women. Breast Cancer Res Treat 2009; 114: 495–501.

42 Buzdar AU, Robertson JF, Eiermann W, Nabholtz JM. An overview of the pharmacology and pharmacokinetics of the newer generation aromatase inhibitors anastrozole, letrozole, and exemestane. Cancer 2002; 95: 2006–16.

43 McCloskey EV, Hannon RA, Lakner G, Fraser WD, Clack G, Miyamoto A, *et al.* Effects of third generation aromatase inhibitors on bone health and other safety parameters: results of an open, randomised, multicentre study of letrozole, exemestane and anastrozole in healthy postmenopausal women. Eur J Cancer 2007; 43: 2523–31.

44 Zhang J, Jiang Z, Zhang L. Effect of triptolide on aromatase activity in human placental microsomes and human placental JEG-3 cells. Arzneimittelforschung 2011; 61: 727–33.

45 Hecker M, Newsted JL, Murphy MB, Higley EB, Jones PD, Wu R, *et al.* Human adrenocarcinoma (H295R) cells for rapid *in vitro* determination of effects on steroidogenesis: hormone production. Toxicol Appl Pharmacol 2006; 217: 114–24.

46 Wood PM, Woo LW, Humphreys A, Chander SK, Purohit A, Reed MJ, *et al.* A letrozole-based dual aromatase-sulphatase inhibitor with *in vivo* activity. J Steroid Biochem Mol Biol 2005; 94: 123–30.

47 Gervais M, Tan L. 6-Hydroximinoandrostenedione, a new specific inhibitor of estrogen biosynthesis and its effect on T47D human breast cancer cells. Anticancer Res 1993; 13: 383–8.

48 Long BJ, Tilghman SL, Yue W, Thiantanawat A, Grigoryev DN, Brodie AM. The steroidal antiestrogen ICI 182,780 is an inhibitor of cellular aromatase activity. J Steroid Biochem Mol Biol 1998; 67: 293–304.

49 Hartman J, Lindberg K, Morani A, Inzunza J, Strom A, Gustafsson JA. Estrogen receptor beta inhibits angiogenesis and growth of T47D breast cancer xenografts. Cancer Res 2006; 66: 11207–13.

50 Sadekova SI, Tan L, Chow TY. Identification of the aromatase in the breast carcinoma cell lines T47D and MCF-7. Anticancer Res 1994; 14: 507–11.

51 Ryde CM, Nicholls JE, Dowsett M. Steroid and growth factor modulation of aromatase activity in MCF7 and T47D breast carcinoma cell lines. Cancer Res 1992; 52: 1411–5.

52 Brooks JD, Thompson LU. Mammalian lignans and genistein decrease the activities of aromatase and 17beta-hydroxysteroid dehydrogenase in MCF-7 cells. J Steroid Biochem Mol Biol 2005; 94: 461–7.